Geoinformatics, vol.10, no.3, pp.129-142, 1999

ARTICLE

FACTORS CONTROLLING PRECISION OF 3D STRAIN ANALYSIS USING ELLIPSOIDAL PASSIVE MARKERS

Daigoro HAYASHI

Department of Physics and Earth Sciences, University of the Ryukyus, Nishihara, Okinawa, 903-0213, Japan.
E-mail: daigoro@sci.u-ryukyu.ac.jp

(Received: 24 July 1998; Accepted: 28 June 1999)

Abstract : Three series of model are prepared to examine what factor controls the precision of strain where the axial ratio of initial strain marker ellipsoids is assumed to scatter as a normal distribution. The average method is used to analyze the 3D strain of the present simulation. Three series of model are produced to test three factors; (1) sample size of markers, (2) mean of axial ratio of makers and (3) standard deviation of axial ratio of markers. The simulation is performed in three deformational fields; pure shear of plane strain, isochoric transpression and simple shear of plane strain. Results of the simulation are; (1) When the sample size of the initial strain marker ellipsoids is large, the precision of strain analysis is high. But the precision does not change over 300 sample size. (2) When the mean of axial ratio of the initial strain marker ellipsoids closes to unity, the precision of strain analysis is high. (3) If the standard deviation of axial ratio of the initial strain marker ellipsoids becomes smaller than unity, the precision of strain analysis becomes high. (4) These results hold almost in the same way for the three deformational fields. The exception is; the strain precision becomes high during the progress of deformation under the transpression and the simple shear, though the precision does not change during deformation under the pure shear.

Key words : Precision, 3D strain anaysis, Ellipsoidal passive marker, Average method

1. Introduction

Techniques to analyze strain have been developed by many researchers since Cloos (1947) did. Methods of strain analysis are divided into the orientation method and the shape method. The orientation method was developed by Sanderson (1977), Fry (1979) and Panozzo (1984). Since passive ellipsoids are assumed as strain markers, the discussion in this paper is limited to the shape method.

The shape method comprises the graphic method and the algebraic method. The graphic method includes the shape factor grid method (Elliott,1970) and R_f/ϕ method (Ramsay,1967; Dunnet,1969; Dunnet and Siddans,1971; Lisle,1977,1985). The algebraic method is composed of the method by Matthews *et al.*(1974) and the average method (Shimamoto and Ikeda,1976; Wheeler,1986). The R_f/ϕ method has such defects that it is subjective and time consuming because of using graphs. The algebraic methods have no such defects though the method by Matthews *et al.* needs other data such as a direction of long axis of strain. I believe the averaged method is most convenient for the strain analysis of both 2D and 3D using passive ellipsoidal (elliptical) markers, because of its theoretical soundness and simplicity. The method was first described by Shimamoto and Ikeda (1976) and was precisely studied by Wheeler(1986).

On the other hand, regarding the precision of strain analysis, as long as I know, Siddans (1980) is the only one example. His simulation is performed as ; (1) 100 randomly oriented initial ellipsoids with constant axial ratio were set up. (2) They were deformed homogeneously to derive R_f/ϕ data. (3) The R_f/ϕ data were analyzed in five ways. Two ways are the calculation of simple algebraic means of R_f such as arithmetic and harmonic means. The other three ways are the method by the R_f/ϕ, the method by Matthews *et al.*(1974) and the average method (Shimamoto and Ikeda, 1976). Siddans' simulation can say which technique is best to calculate strain but nothing more. His simulation did not give what the factor of precision of strain analysis is.

In the present paper I have simulated three series of strain marker model for three deformational fields containing coaxial and non-coaxial fields to examine the factor of precision of 3D strain analysis. The shape of strain marker is assumed to be ellipsoidal. Suspected factors which affect precision are (1) the sample size of strain markers, (2) the mean of the axial ratio (R_i)

of strain markers, (3) the standard deviation of R_i and (4) type of deformational field; pure shear, isochoric transpression and simple shear.

The simulation is performed as follows. (1) Several hundred randomly oriented marker ellipsoids are produced. Their axial ratio $R_i \left(=\frac{X_i}{Z_i}\right)$ shows a normal distribution. (2) They are deformed homogeneously in three deformational fields with different W_k. (3) Fabric ellipsoid is calculated by averaging the shape tensor component of maker ellipsoids. (4) Fabric and strain ellipsoids are compared to calculate the difference of distance from its center to its surface point between both ellipsoids.

2. Average method

The average method is explained below, because the simulation that will be described in the paper is clearly understood if we recognize the relation between the fabric ellipsoid and the strain ellipsoid as illustrated in Fig.1. I use different definition of the terms "shape tensor" and "fabric ellipsoid" from the definition of Wheeler (1986) because Wheeler's definition is confusional. Mathematical symbols are referred to the Notation.

When an ellipsoid is described in its vector form

$$\mathbf{x}^T A \mathbf{x} = 1,$$

I call A as "shape tensor" of the ellipsoid and the shape tensor is already normalized by cubic root of determinant of A because we are always interested to the shape of the ellipsoid.Let's consider plural ellipsoids whose shape tensors are A_i ($i = 1,2,\cdots, n$). We add each component of A_i and normalize the resultant tensor to obtain an average tensor. I call the average tensor as "the shape tensor of fabric ellipsoid".

Consider the randomly oriented passive marker ellipsoids whose equations are

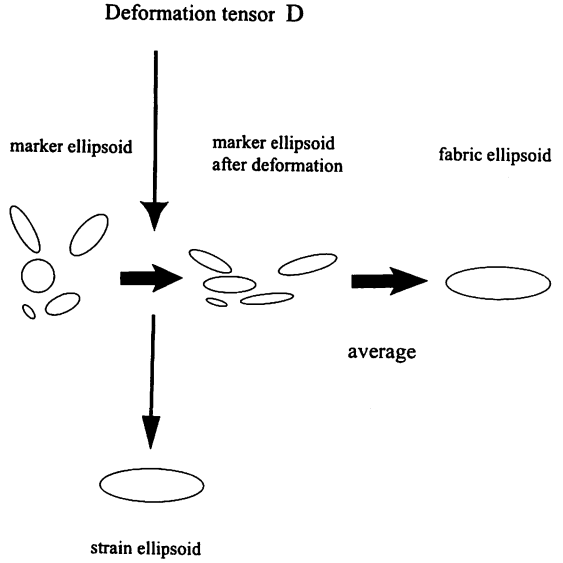

Fig.1 Relation between fabric ellipsoid and strain ellipsoid

$$\mathbf{x}^T A_i \mathbf{x} = 1 \quad (i = 1,2,\cdots, n).$$

When they are transformed by a deformation tensor D ($\mathbf{x}'=D\mathbf{x}$), the marker ellipsoids are written as

$$(D^{-1}\mathbf{x}')^T A_i (D^{-1}\mathbf{x}') = 1.$$

$$(\mathbf{x}')^T (D^{-1})^T A_i D^{-1} \mathbf{x}' = 1.$$

Averaging the shape tensor as

$$B = \text{average}\left\{(D^{-1})^T A_i D^{-1}\right\} = (D^{-1})^T \text{average}\{A_i\}\, D^{-1},$$

B is the shape tensor of fabric ellipsoid according to the former definition.

If the initial marker ellipsoids are averaged to a sphere, their axes were randomly oriented before deformation. If this is the case, the average of the initial shape tensor of the markers is a unit tensor. Thus the average tensor B is

$$B = (D^{-1})^T \text{average}\{A_i\}\, D^{-1} = (D^{-1})^T I D^{-1} = (DD^T)^{-1}$$

The shape tensor of the fabric ellipsoid is $(DD^T)^{-1}$.

On the other hand, consider the deformation of a unit sphere

$$\mathbf{x}^T \mathbf{x} = 1$$

which is transformed by D as follows.

$$(D^{-1}\mathbf{x}')^T (D^{-1}\mathbf{x}') = 1$$
$$(\mathbf{x}')^T (D^{-1})^T D^{-1} \mathbf{x}' = 1$$
$$(\mathbf{x}')^T (DD^T)^{-1} \mathbf{x}' = 1$$

This must be a strain ellipsoid. Thus, if the initial marker ellipsoids are randomly oriented, their fabric ellipsoid coincides to the strain ellipsoid.

Notation	Explanation of symbols
X	length of long axis of strain ellipsoid
Y	length of intermediate axis of strain ellipsoid
Z	length of short axis of strain ellipsoid
$R=\frac{X}{Z}$	axial ratio of strain ellipsoid
X_i	length of long axis of marker ellipsoid
Y_i	length of intermediate axis of marker ellipsoid
Z_i	length of short axis of marker ellipsoid
$R_i=\frac{X_i}{Z_i}$	axial ratio of marker ellipsoid
n	sample size
m	mean of R_i
σ	standard deviation of R_i
D	deformation tensor = position gradient tensor
$(DD^T)^{-1}$	shape tensor of strain ellipsoid
W_k	kinematic vorticity number
L_{ij}	velocity gradient tensor
I	unit tensor

3. Deformational field

According to Ramberg (1975), McKenzie and Jackson (1983), Tikoff and Fossen (1993) and others, a deformation tensor is derived from a velocity gradient tensor. Instantaneous movement is described as

$$\dot{x}_i = L_{ij} x_j$$

where L_{ij} is the velocity gradient tensor

$$L = \begin{bmatrix} \dot{\varepsilon}_x & \dot{\gamma}_{xy} & \dot{\gamma}_{xz} \\ 0 & \dot{\varepsilon}_y & \dot{\gamma}_{yz} \\ 0 & 0 & \dot{\varepsilon}_z \end{bmatrix}.$$

The kinematic vorticity number (Truesdell,1953) is written as

$$W_k = \frac{\sqrt{(\dot{\gamma}_{yz})^2 + (\dot{\gamma}_{xz})^2 + (\dot{\gamma}_{xy})^2}}{\sqrt{2(\dot{\varepsilon}_x^2 + \dot{\varepsilon}_y^2 + \dot{\varepsilon}_z^2) + (\dot{\gamma}_{yz})^2 + (\dot{\gamma}_{xz})^2 + (\dot{\gamma}_{xy})^2}}$$

In the present simulation I choose three deformational fields as follows.

(1) Pure shear and plane strain rate is illustrated in Fig.2. Since the components except for $\dot{\varepsilon}_x$ and $\dot{\varepsilon}_z$ are zero, the velocity gradient tensor is

$$L = \begin{bmatrix} \dot{\varepsilon}_x & 0 & 0 \\ 0 & 0 & 0 \\ 0 & 0 & \dot{\varepsilon}_z \end{bmatrix} = \begin{bmatrix} 0.01 & 0 & 0 \\ 0 & 0 & 0 \\ 0 & 0 & -0.01 \end{bmatrix}$$

and $W_k = 0$.

Thus the corresponding deformation tensor of a steady state is

$$D = \begin{bmatrix} \exp(\dot{\varepsilon}_x t) & 0 & 0 \\ 0 & 1 & 0 \\ 0 & 0 & \exp(\dot{\varepsilon}_z t) \end{bmatrix}$$

where $\dot{\varepsilon}_x + \dot{\varepsilon}_z = 0$.

In this simulation $\dot{\varepsilon}_x$ takes 0.01 and the marker ellipsoids are deformed 100 times varying the variable t from 1 to 100, while R moves 1.0202 to 7.38906. R means the axial ratio of the strain ellipsoid during deformation.

(2) Isochoric transpression is shown in Fig.3.

The velocity gradient tensor is

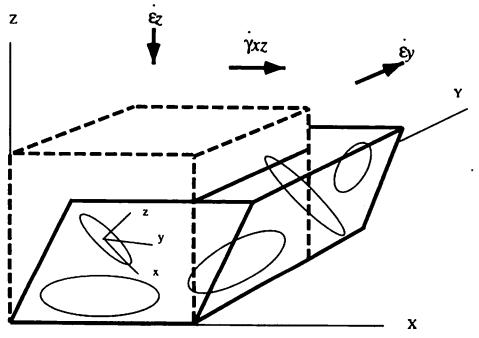

Fig.3 Isochoric transpression

$$L = \begin{bmatrix} 0 & 0 & \dot{\gamma}_{xz} \\ 0 & \dot{\varepsilon}_y & 0 \\ 0 & 0 & \dot{\varepsilon}_z \end{bmatrix} = \begin{bmatrix} 0 & 0 & 0.01 \\ 0 & 0.01 & 0 \\ 0 & 0 & -0.01 \end{bmatrix}$$

and $W_k = 0.4472$.

A steady state deformation tensor D is

$$D = \begin{bmatrix} 1 & 0 & \frac{\dot{\gamma}_{xz}}{\dot{\varepsilon}_z}\left|\exp(\dot{\varepsilon}_z t) - 1\right| \\ 0 & \exp(\dot{\varepsilon}_y t) & 0 \\ 0 & 0 & \exp(\dot{\varepsilon}_z t) \end{bmatrix}$$

where $\dot{\varepsilon}_y + \dot{\varepsilon}_z = 0$.

$\dot{\varepsilon}_y$ takes 0.01, $\dot{\gamma}_{xz}$ takes 0.01 and the marker ellipsoids are deformed 100 times varying the variable t from 1.2 to 120 at interval 1.2, while R moves 1.02684 to 13.5873.

(3) Simple shear and plane strain rate is illustrated in Fig.4.

The velocity gradient tensor is

$$L = \begin{bmatrix} 1 & 0 & \dot{\gamma}_{xz} \\ 0 & 0 & 0 \\ 0 & 0 & 0 \end{bmatrix} = \begin{bmatrix} 0 & 0 & 0.01 \\ 0 & 0 & 0 \\ 0 & 0 & 0 \end{bmatrix}$$

and $W_k = 1$

The deformation tensor of a steady state is

$$D = \begin{bmatrix} 1 & 0 & \dot{\gamma}_{xz} t \\ 0 & 1 & 0 \\ 0 & 0 & 1 \end{bmatrix}.$$

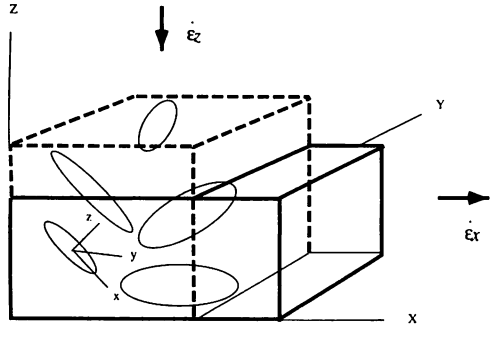

Fig.2 Pure shear and plane strain rate

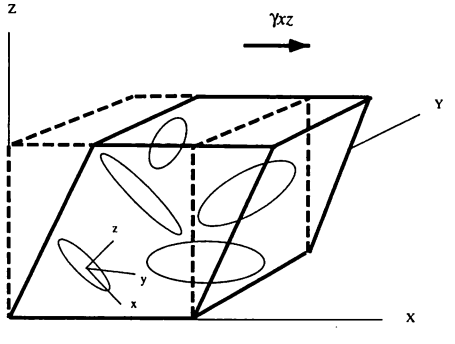

Fig.4 Simple shear and plane strain rate

$\dot{\gamma}_{xz}$ takes 0.01 and the marker ellipsoids are deformed 100 times varying the variable t from 4 to 400 at interval 4, while R moves 1.04081 to 17.9443.

Thus we have three types of deformation tensor by which any marker ellipsoid is deformed in three ways. If the marker ellipsoid before deformation is described as

$$\mathbf{x}^T A_i \mathbf{x} = 1,$$

the marker ellipsoid after deformation becomes

$$(D^{-1}\mathbf{x}')^T A_i (D^{-1}\mathbf{x}') = 1$$

where $\mathbf{x}' = D\mathbf{x}$.

4. Marker ellipsoid

4.1 Property of strain marker

Strain markers are assumed to have the following properties.

(1) Shape of the marker is ellipsoidal.

(2) There is no competency contrast between the marker and the matrix.

(3) Initial principal axes of the marker are randomly oriented.

(4) Markers are homogeneously deformed.

(5) Markers do not change their volume during deformation.

(6) The axial ratio $\left(R_i = \frac{X_i}{Z_i}\right)$ of the markers shows a normal distribution.

The assumptions from (1) to (4) are the same those in the case of two dimensional finite strain analysis using ellipse-shape strain markers. I have supposed that the conditions of (5) and (6) are reasonable for the natural strain markers, if the mean of the normal distribution is near unity.

4.2 Series of model

It is examined how the following three factors affect to the precision of 3D strain analysis, assuming that the axial ratio of the strain markers shows a normal distribution.

(1) Sample size of the strain markers.

(2) Mean of the axial ratio (R_i) of the strain markers.

(3) Standard deviation of R_i.

Three series including twelve models are produced to perform the simulation. Ten models within the twelve's are independent because the model 1 is used repeatedly third times in the different series as a standard model. Three series of model are constructed and simulated for each deformational field; the pure shear, the isochoric transpression and the simple shear. Thus the three types of deformation are also the factors which expect to control the precision of strain.

(1) Series A : The sample size (n) of the marker varies, while the mean (m) and the standard deviation (σ) of the axial ratio (R_i) of the marker are both fixed as unity. The series is composed of four models; model 1, model 8, model 9 and model 10, as described on Table 1a.

(2) Series B : The mean (m) of R_i varies, while the sample size(n) and the standard deviation (σ) are fixed as $n = 100$ and $\sigma = 1$. The series includes four models; model 1, model 5, model 6 and model 7, as shown on Table 1b.

(3) Series C : The standard deviation (σ) of R_i varies, while the sample size (n) and the mean (m) are fixed as $n = 100$ and $m = 1$. The series includes four models; model 1, model 2, model 3 and model 4, as written on Table 1c.

Table 1 Series of strain marker model. n is sample size, m is mean and σ is standard deviation of R_i.

Table 1a Series A

	n	m	σ
model 1	100	1	1
model 8	300	1	1
model 9	600	1	1
model 10	1000	1	1

Table 1b Series B

	n	m	σ
model 1	100	1	1
model 5	100	2	1
model 6	100	5	1
model 7	100	10	1

Table 1c Series C

	n	m	σ
model 1	100	1	1
model 2	100	1	0.8
model 3	100	1	0.5
model 4	100	1	0.2

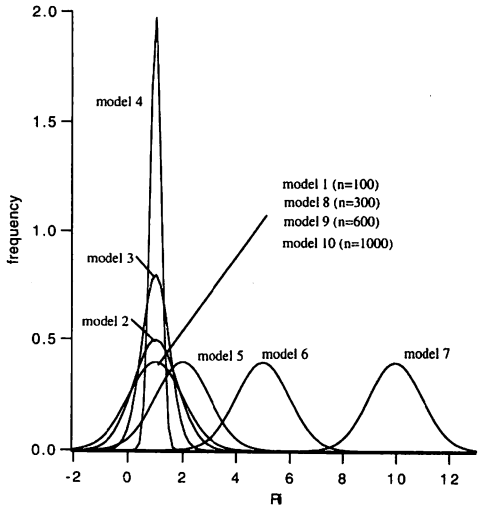

Fig.5 Normal distributions assumed for all models. Curves of models 1, 8, 9 and 10 are same because their m and σ coincide with each other. All curves are defined in the region larger than unity of R_i.

The curves of normal distribution for the ten models are illustrated in Fig.5.

4.3 Normal random number

The axial ratio (R_i) of marker ellipsoids is assumed to the normal random numbers. The normal random numbers are produced from uniform random numbers by the Box and Muller method. Using two uniform random numbers u_i and u_{i+1}, the normal random numbers z_i and z_{i+1} whose mean and standard deviation are m and σ are calculated by the equations.

$$z_i = \sqrt{-2\log u_i}(\cos 2\pi)(u_{i+1})\,\sigma + m$$

$$z_{i+1} = \sqrt{-2\log u_i}(\sin 2\pi)(u_{i+1}) + m$$

4.4 *XZ* diagram of ellipsoid

X, Y and Z are the length of long, intermediate and short axes of an ellipsoid where $X \geq Y \geq Z$. Dividing the inequality $X \geq Y \geq Z$ by Y into $\frac{X}{Y} \geq 1 \geq \frac{Z}{Y}$, we rewrite X instead of $\frac{X}{Y}$ and Z instead of $\frac{Z}{Y}$ because we are interested to the shape of the ellipsoid. Let's define the axial ratio (R) of the ellipsoid as $R = \frac{X}{Z}$, then R means the gradient of a line through the origin (0,0) as illustrated in Fig.6 where X and Z show ordinate and abscissa, respectively. I call the figure "XZ diagram". According to the relation $X \geq Z$, the defined region of the possible point (Z, X) is limited to the upper left rectangular part which is bounded by $X = 1$ and $Z = 1$.

4.5 Marker point on X_iZ_i diagram

A marker ellipsoid is shown as a point on X_iZ_i diagram where X_i and Zi are ordinate and abscissa. The point is called "marker point". The intersection of a line X_i=R_iZ_i and a line X_i=1 is P_1 and the intersection of a line X_i=R_iZ_i and Z_i=1 is P_2 on the X_iZ_i diagram (Fig.7). The distance between P_1 and P_2 is assumed to be unity. We define arbitrarily a marker point (Z_i, X_i) by producing a random number between 0 to 1 as follows. On the X_iZ_i diagram, let rewrite the variable Z_i to x as abscissa and variable X_i to y as ordinate, and R_i to m. Since the point P_1 is the intersection of both the lines

$$\begin{cases} y = mx \\ y = 1 \end{cases},$$

we have the coordinate of P_1 as $\left(\frac{1}{m}, 1\right)$. Similarly for the point P_2 which is the intersection of

$$\begin{cases} y = mx \\ x = 1 \end{cases},$$

we have P_2 as (1, m). Therefore, when we divide equally the distance between P_1 and P_2 into n parts, both increments of x and y are

$$\begin{cases} x_{inc} = \dfrac{\left(1 - \frac{1}{m}\right)}{n} \\ y_{inc} = \dfrac{m-1}{n} \end{cases}.$$

We have the coordinate (x_k, y_k) of the kth point as

$$\begin{cases} x_k = \dfrac{1}{m} + \left(1 - \dfrac{1}{m}\right)\dfrac{k}{n} \\ y_k = 1 + (m-1)\dfrac{k}{n} \end{cases}.$$

In order to produce random points ranging between P_1 and P_2 on the line $y = mx$, the value of k/n is exchanged to a random number between 0 to 1. Calculating the coordinate (x_k, y_k) in this way, the (x_k, y_k) could be the coordinate of a random marker point (Z_i, X_i). Since $Y_i = 1$ on the X_iZ_i diagram, the principal axial lengths of the marker ellipsoid are obtained as X_i, 1 and Z_i.

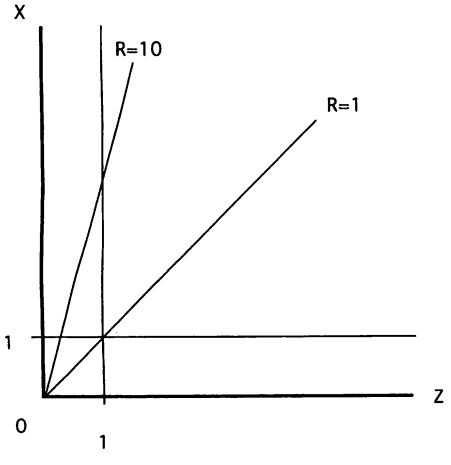

Fig.6 XZ diagram where X and Z mean the long and the short axial length of a strain ellipsoid.

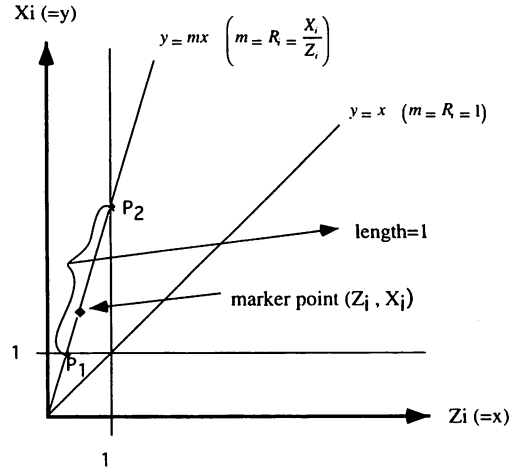

Fig.7 X_iZ_i diagram. Y_i is defined to be unity. P_1 is the intersection of a line $y = mx$ and a line $y = 1$. P_2 is the intersection of $y = mx$ and $x = 1$. The distance between P_1 and P_2 is defined as unity.

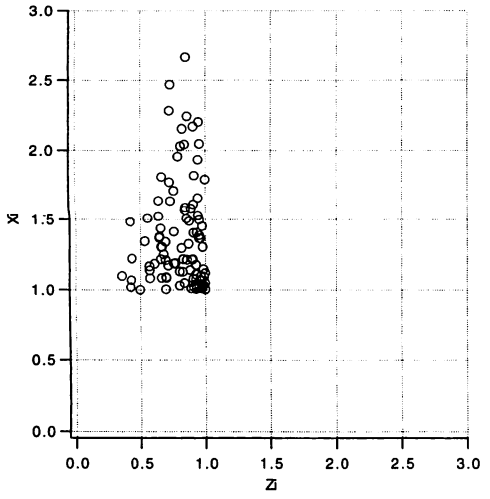

Fig.8 Distribution of initial marker points of the model 1 ($n = 100$, $m = 1$ and $\sigma = 1$) on X_iZ_i diagram as an example. It is noticeable that all the points are distributed within the triangular region delimited by three lines, $X_i = 1$, $Z_i = 1$ and $X_i = kZ_i$.

An example of the distribution of initial marker points on the X_iZ_i diagram is illustrated in Fig.8.

4.6 Random distribution of principal axes of a marker ellipsoid

Producing the marker ellipsoid whose axes are randomly oriented is same as producing an orthogonal *xyz* system that rotates randomly around the present orthogonal *XYZ* coordinate system. If the direction of the x axis is indicated by the Euler angle (α , β , γ), we have

$$\cos^2\alpha + \cos^2\beta + \cos^2\gamma = 1.$$

The formula is changed into

$$\cos\gamma = \pm\sqrt{1-\cos^2\alpha-\cos^2\beta}\ .$$

The x, y and z axes are calculated by the following procedure.

(1) Define α and β randomly.

(2) Define γ using the above formula. Then x axis is obtained.

(3) Repeat the calculation from (1) to (2), and define the other axis which is called p axis.(4) Define y axis as the intersection of two planes whose poles are x and p.

(5) Define z axis as the vector product of x and y axes.

4.7 Representation of a marker ellipsoid in the *XYZ* system

A marker ellipsoid described in the orthogonal *xyz* system is

$$\mathbf{x}^T A_i \mathbf{x} = 1$$

where

$$A_i = \begin{bmatrix} \frac{1}{X_i^2} & 0 & 0 \\ 0 & 1 & 0 \\ 0 & 0 & \frac{1}{Z_i^2} \end{bmatrix}$$

and notice $Y_i = 1$.

The equation is transferred to the equation that is presented in the other coordinate *XYZ* system if we know the transform tensor between the two coordinate systems. The transform tensor is supposed here as

$$\mathbf{x} = T\mathbf{X}$$

where

$$T = \begin{bmatrix} \cos\theta_{11} & \cos\theta_{12} & \cos\theta_{13} \\ \cos\theta_{21} & \cos\theta_{22} & \cos\theta_{23} \\ \cos\theta_{31} & \cos\theta_{32} & \cos\theta_{33} \end{bmatrix}.$$

The direction cosine of x axis is ($\cos\theta_{11}$, $\cos\theta_{12}$, $\cos\theta_{13}$), and those of y and z axes are ($\cos\theta_{21}$, $\cos\theta_{22}$, $\cos\theta_{23}$) and ($\cos\theta_{31}$, $\cos\theta_{32}$, $\cos\theta_{33}$), respectively as illustrated in Fig.9. The marker ellipsoid described in the *XYZ* system is

$$(T\mathbf{X})^T A_i (T\mathbf{X}) = 1.$$

$$\mathbf{X}^T (T^T A_i T)\mathbf{X} = 1.$$

$$\mathbf{X}^T B_i \mathbf{X} = 1.$$

where $B_i = T^T A_i T$.

5. Shape error

Regarding three series of model including twelve models described in the section 4.2, the fabric ellipsoid is calculated by averaging the shape tensor component of marker ellipsoids. We cannot clearly recognize the difference between the fabric and the strain ellipsoids , for example, on a normalized Flinn diagram* because the difference is small. Thus I use "shape error".

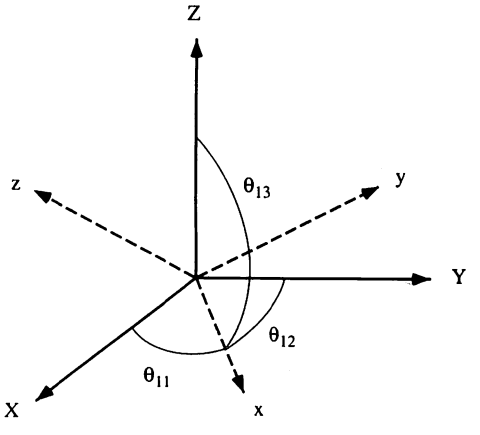

Fig.9 Two orthogonal coordinate systems, *XYZ* and *xyz*.

* The normalized Flinn diagram is the Flinn diagram where the length of Y axis is defined unity. As a result the abscissa is $\frac{1}{z}$ and the ordinate is X.

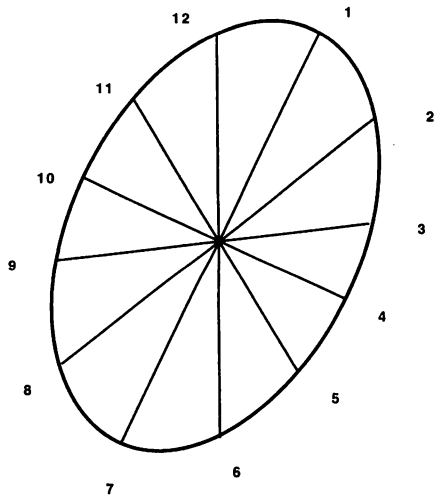

Fig.10 Twelve direction points on one of the principal section of an strain ellipsoid. They divide the section ellipse at interval of 30° .The direction of 1 and 7 coincides with the long axis and that of 4 and 10 coincides with the short axis of the strain ellipsoid.

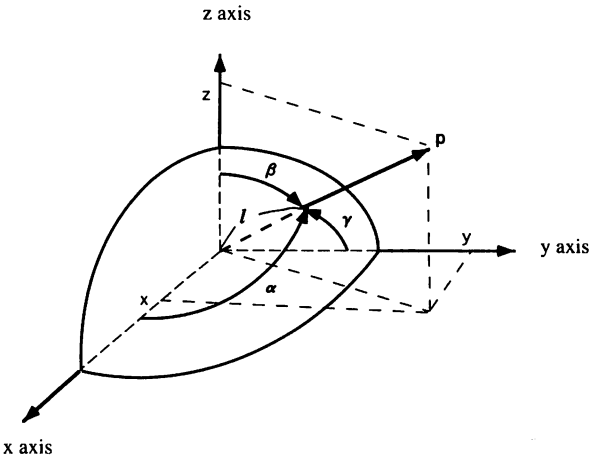

Fig.11 A direction vector **p** is denoted by Euler angle (α , β , γ) and its coordinate is (x, y, z). An intersection between **p** and the surface of the ellipsoid shows distance l from the origin.

The shape error is the concept which measures the difference between a fabric ellipsoid and a strain ellipsoid. The concept was originally created by Hayashi(1995) calling "normalized distance" and is described briefly as follows. Both concepts of the shape error and the normalized distance are similar but different, because the shape error use the principal plane of strain ellipsoid but the normalized distance use the plane which is arbitrarily chosen at the measurement of strain in field.

The figure 10 illustrates one of the principal plane of a strain ellipsoid. If we divide one twelfth every 30° the arc of the section ellipsoid from one of the principal axes (point 1), we would locate 36 points on the three principal planes. I call the 36 points "36 directions" since they are the directions defined in the xyz coordinate. In Fig.11, we represent any vector **p** as

$$\mathbf{p} = \begin{pmatrix} x \\ y \\ z \end{pmatrix}.$$

We have the next relation with regard to any vector **p**

$$|\mathbf{p}| = \sqrt{x^2 + y^2 + z^2}$$

where

$$\cos\alpha = \frac{x}{|\mathbf{p}|}, \quad \cos\beta = \frac{y}{|\mathbf{p}|}, \quad \cos\gamma = \frac{z}{|\mathbf{p}|}.$$

Suppose that **p** lies on the ellipsoid, the equation holds

$$(x\ y\ z)\begin{bmatrix} a & b & c \\ & d & e \\ sym & & h \end{bmatrix}\begin{pmatrix} x \\ y \\ z \end{pmatrix} = 1.$$

The equation is expanded as

$$ax^2 + abxy + 2czx + dy^2 + 2eyz + hz^2 = 1.$$

Suppose the distance between the surface point and the center of the ellipsoid to be l. The surface point is the point that intersects the vector **p** and the surface of the ellipsoid. We have relations

$$x = l\cos\alpha, \quad y = l\cos\beta, \quad z = l\cos\gamma$$

and

$$l^2(a\cos^2\alpha + 2b\cos\alpha\cos\beta + 2c\cos\gamma\cos\alpha + d\cos^2\beta + 2e\cos\beta\cos\gamma + h\cos^2\gamma) = 1.$$

The distance (E_s) of a point (P_s) was calculated that lies on the surface of the strain ellipsoid measured from its center by using the above equation. The distance (E_f) of a point (P_f) was calculated that lies on the surface of the fabric ellipsoid measured from its center. If the direction of both the points P_s and P_f is same, the difference between E_f and E_s are denoted E_{fs} ($=E_f - E_s$). When E_{fs} is divided by E_s,I call it N_{fs}. Since N_{fs} is the value that is the normalized distance between a surface point of the strain ellipsoid and that of the fabric ellipsoid, I call N_{fs} "shape error".

The figure 12 shows the shape error of the 36 directions at R=1.0202 for the model 1 in pure shear. The 36 direction number is taken as abscissa and the shape error (N_{fs}) as ordinate. The line N_{fs}=0 indicates the surface of the strain ellipsoid. The open circles represent the shape error (N_{fs}) of the 36 directions. When the open circle approaches toward the line N_{fs}=0, the fabric ellipsoid closes to the strain ellipsoid.

6. Comparison of fabric ellipsoid and strain ellipsoid

Strain markers of each model have suffered 100 stages of deformation recorded by the axial ratio (R). R runs from 1.0202 to 7.38906 in pure shear; R varies from 1.02684 to 13.5873 in

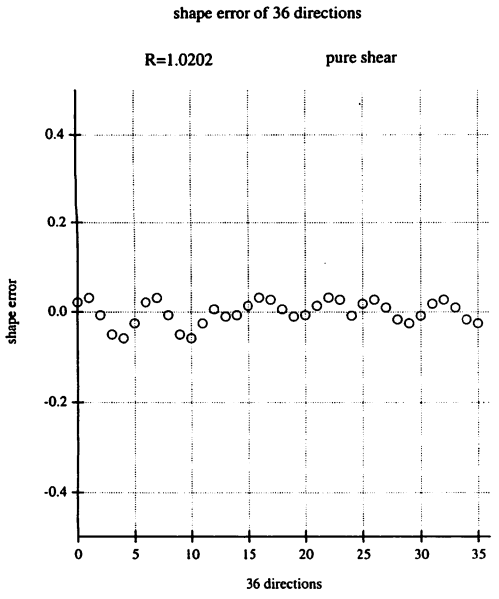

Fig.12 Shape error (N_{fs}) of 36 directions at R = 1.0202 for the model 1 in pure shear. N_{fs} = 0 means the surface of a strain ellipsoid.

transpression, and R moves from 1.04081 to 17.9443 in simple shear. The mean and the standard deviation of the shape error of the 36 directions in every stage of deformation are calculated. The deviation range of the models deformed in pure shear is plotted taking the strain axial ratio (R) as abscissa and the shape error (N_{fs}) as ordinate in Fig.13. The deviation range of the 36 directions for each R is drawn by the parallel line to the ordinate axis in the figure. The center of the parallel line indicates the mean of N_{fs} of the 36 directions. The length of the line equals to two times of the standard deviation of N_{fs} of the 36 directions.

Regarding the series A, we can see from Fig.13a that when the sample size of marker ellipsoids increases from 100 to 300, the deviation range of the 36 directions becomes narrow. The strain precision becomes higher in this order. On the other hand the deviation range does not change among the sample size 300, 600 and 1000. There are no change of strain precision for more than 300 sample size.

For the series B, we know from Fig.13b that when the mean of the axial ratio (R_i) of initial marker ellipsoids increases from 1 to 10, the deviation range grows wider. The strain precision becomes lower in this order.

As regard to the series C, we agree from Fig.13c that when the standard deviation of R_i decreases from 1 to 0.2, the deviation range becomes narrow. The strain precision becomes higher in this order.

The figures 14 and 15 show the deviation ranges of the models deformed in the isochoric transpression and the simple shear, respectively. The graphs of the deviation range are truncated at R=10. Three tendencies of the result for the pure shear hold almost same in other deformation types. There are no dif-

a : Series A.

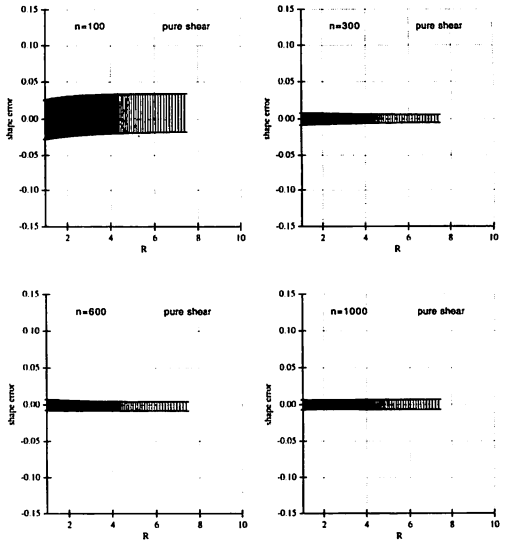

b : Series B.

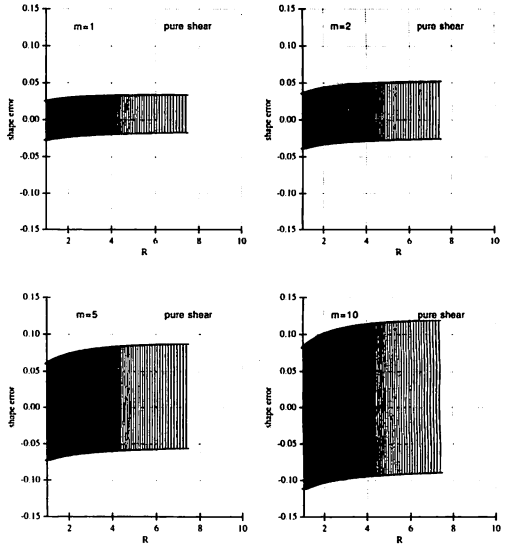

c : Series C.

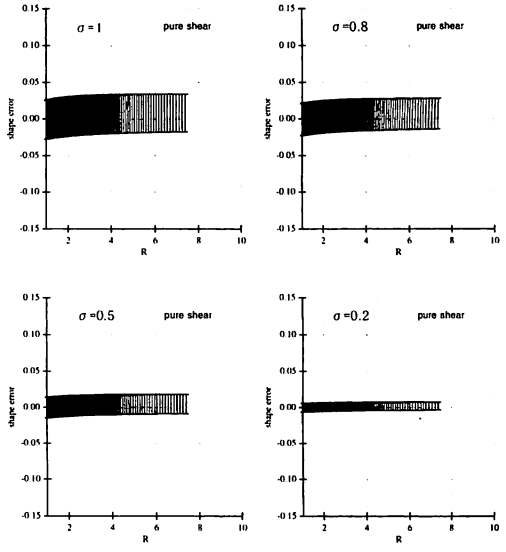

Fig.13 Deviation range of 36 directions indicated for 100 stages of strain axial ratio R (abscissa). Ordinate is taken to the shape error. R varies from 1.0202 to 7.38906.

a : Series A.

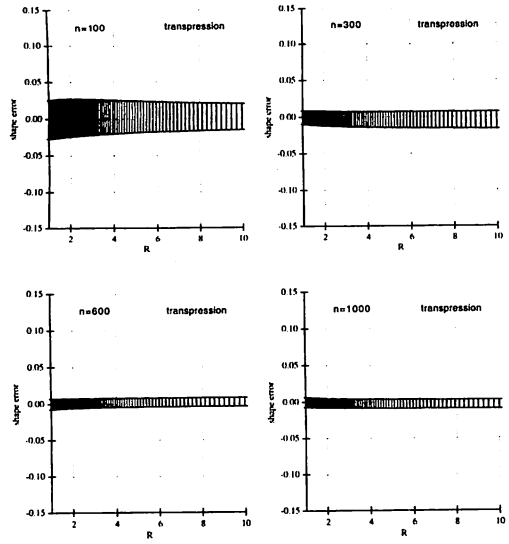

b : Series B.

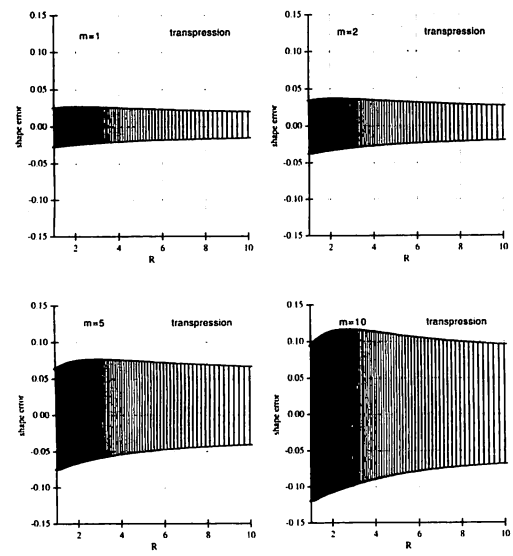

c : Series C.

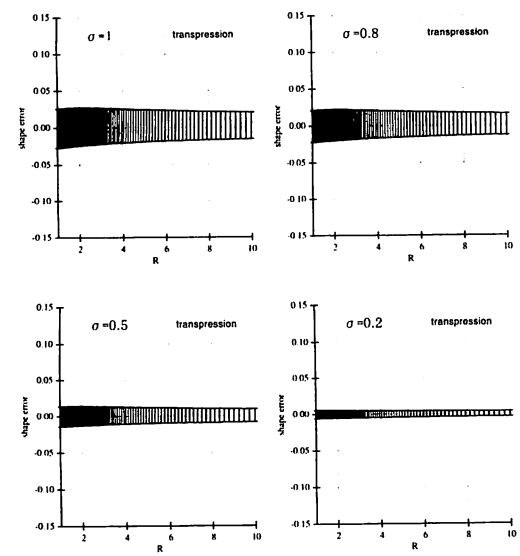

Fig.14 Deviation range of 36 directions indicated for 100 stages of strain axial ratio R (abscissa). Ordinate is taken to the shape error. R varies from 1.02684 to 13.5873 though R axis is truncated at 10.

a : Series A.

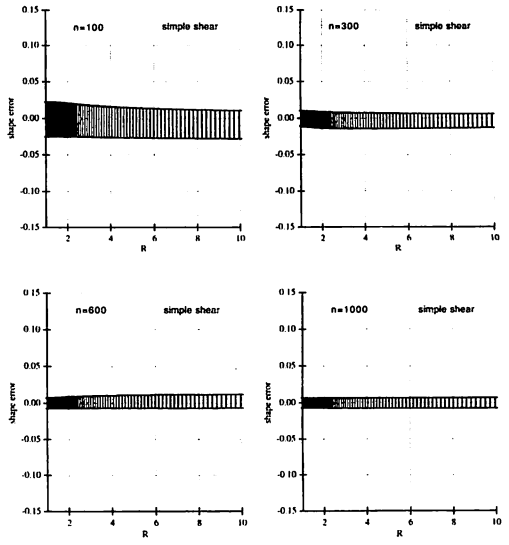

b : Series B.

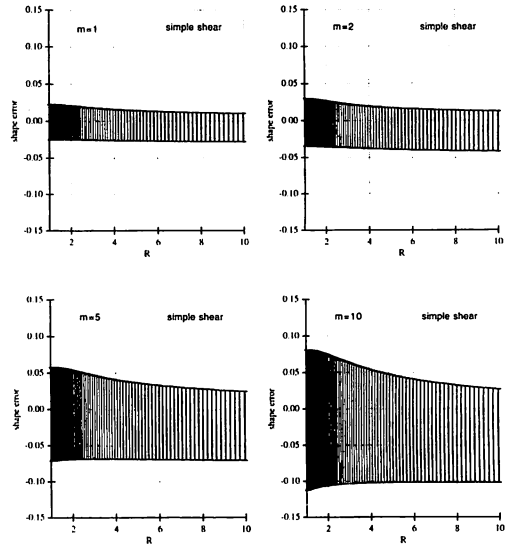

c : Series C.

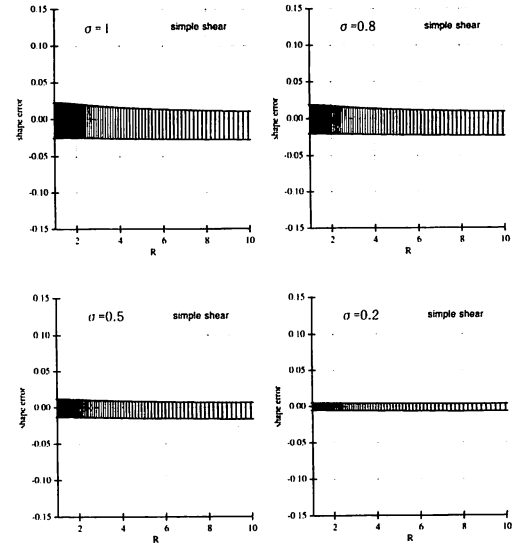

Fig.15 Deviation range of 36 directions indicated for 100 stages of strain axial ratio R (abscissa). Ordinate is taken to the shape error. R varies from 1.04081 to 17.9443 though R axis is truncated at 10.

ferences of precision of strain among three deformational fields, except for the increasing tendency of the strain precision progressing deformation in the transpression and the simple shear.

7. Discussion

7.1 Application to the naturally deformed rocks

There are several kinds of strain markers in naturally deformed rocks, *e.g.* quartz grain in sandstone (Hayashi,1988,1989; Couzens and Dunne,1994), pebble in conglomerate (Lisle,1984), porphyroblast in metamorphic rock (Lacassin and van den Driessche,1983) and xenolith in granite (Ramsay,1967). Other markers such as reduction spot (Ramsay,1967), ooid (Cloos,1947) and lapillus (Oertel,1970; Helm and Siddans,1971) are not frequently seen than the former markers but are adopted more precise markers.

The assumptions for the simulation of the strain precision in the paper are;

(1) Shape of markers is ellipsoid.
(2) No competency contrast between markers and matrix.
(3) Principal direction of marker ellipsoids is random.
(4) Marker ellipsoids suffer no volume change.
(5) Axial ratio of marker ellipsoids shows a normal distribution.

Although these conditions are so strict that no marker stated above satisfies them all, such markers as reduction spot, ooid and lapillus satisfy the conditions (1), (2) and (4). While the condition (3) is not satisfied except for horizontal randomness because these markers lie under the gravity. However the simulation could be performed if we measure the principal directions of lapilli from the same formation of lapilli tuff in the undeformed region and make them as the input data.

Similary, the condition (5), R_i shows a normal distribution, is not expected in general. If we measure the distribution of R_i of ooid from the same formation of oolite limestone of undeformed area and let them as the input data, we could simulate properly to obtain strain. In this case, the distribution of R_i is not necessarily presented as an explicit function. Modifying the conditions (3) and (5) in this way, the reduction spot, ooid and lapillus could be used as a good strain marker.

7.2 Future possibility

On the natural situation stated above, *e.g.* on the strain analysis of sandstone beds using quartz grain as a marker, the competency contrast is the important condition to be overcome. Since the average method cannot be used, we should take the other methods; *e.g.* the Fry method (Fry,1979) is the prominent alternative. If we obtain the strain distribution using the Fry method, however, the value of strain is difficult to accept. Because no estimation of strain precision of the Fry method have been performed. The present simulation, which is the powerful method to estimate strain precision, can evaluate the precision of the Fry method.

7.3 Large strain

Since the large strain where $R\left(=\frac{X}{Y}\right)$ over 20 occures in natural shear zones, it is necessary to check that the present simulation method can treat with large strain. Thus, with regard to the deformation of the simple shear of model 1 where n = 100, m = 1 and σ = 1, the simulation is performed till R reaches to 38. The result is shown on Fig.16 from which we agree the present simulation can handle such large strain as 40.

7.4 Error correction

The definition of shape error is $N_{fs}=\frac{E_f-E_s}{E_s}$.

If N_{fs} is positive, the fabric ellipsoid is larger than the strain ellipsoid along the direction, and vice versa.

As shown Fig.13,14 and 15, the shape error means the deviation range of N_{fs} on the 36 directions and indicates the difference between the fabric ellipsoid and the strain ellipsoid.

One wants to use these figures to correct errors of strain to the true value.In fact, the figures could be used as a correction diagram to obtain true strain, if the initial conditions of markers are matched together with the simulation and the nature. In practice, this correction has little meaning, because the value of errors is too small. In fact we cannot present them in the Flinn graph. The errors are one order smaller than the errors commonly discussed. It is properly said that the fabric ellipsoid could be taken as the strain ellipsoid in the present simulation except for the case m = 5 and m = 10, if the initial conditions of markers are same in the simulation and the nature.

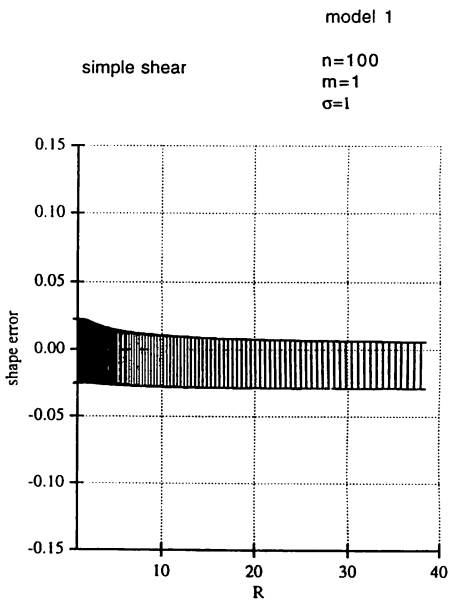

Fig.16 Deviation range of 36 directions indicated for 100 stages of strain axial ratio R (abscissa). Ordinate is taken to the shape error. R varies from 1.06183 to 37.9737.

Appendix

The average method is applied to analyze strain to the general deformational field such as coaxial and non-coaxial deformations. The most important point which justifies the simulation is the randomness of the marker ellipsoids. The randomness regards to both the axial direction and the axial length of the marker ellipsoids. Four tests are described here how the distribution of the initial markers fits with the assumed statistical distribution, such as the normal distribution and the uniform distribution.

A.1. Randomness test of normal random number

The present simulation assumes that the axial ratio (R_i) of initial marker ellipsoids shows a normal distribution. We should examine how the distribution of the normal random number fits with the normal distribution.

The χ^2 test (test of goodness of fitness) is used for the examination. The χ^2 test is the test whether an empirical distribution (sample distribution) fits well with a theoretical distribution (distribution of population).

Considering an empirical and a theoretical distribution as $\{f_i\}$ and $\{f_i^*\}$ (i = 1 to k), the formula of χ^2 is defined as follows.

$$\chi^2 = \sum_{i=1}^{k} \frac{(f_i - f_i^*)^2}{f_i^*}$$

When we compare the values of χ^2 and χ^2_α, and if we have

$$\chi^2 > \chi^2_\alpha$$

, then we should abandon the hypothesis at α. The hypothesis is "sample is a random sample of population". χ^2_α means the χ^2 value at the level of significance α and at the freedom $\phi = k - 1$.

In the present paper there are four sample sizes, n =100, 300, 600 and 1000. The normal distribution of $m = 0$ and $\sigma = 1$ is called "standard normal distribution". Since any normal distribution is derived from the standard normal deistribution by varing the mean and the standard deviation, the standard normal distributions of four sample size are examined instead of all the normal distributions of various means and of various standard deviations. If the variable of normal distribution is unlimited, this is true. In the present case R_i is defined on either the domain $[m-3\sigma, m+3\sigma]$ or the domain $[1, m+3\sigma]$ if $m-3\sigma < 1$. Thus the χ^2 for all the models should be calculated.

The equation of the normal distribution $N(m, \sigma^2)$ is represented as

$$\phi = \frac{1}{\sqrt{2\pi}\sigma} \exp\left[-\frac{(x-m)^2}{2\sigma^2}\right]$$

where x is the variable. The probability of the normal distribution within the range $[x_1, x_2]$ is calculated by

$$\int_{x_1}^{x_2} \phi(x)\, dx$$

which is equal to the frequency of the theoretical distribution. The χ^2 values are calculated for all the models as shown on Table 2 where the freedom is 7.

The value of χ^2_α is shown on Table 3. χ^2_α is the value of χ^2 at the level of significance (α) where α varies from 0.99 to 0.005 and the freedom is 7. We know from the tables that all the χ^2 values calculated for ten models are small enough compared to the χ^2_α value. The normal random number thus produced fits well with normal distribution.

A.2. Randomness test of uniform random number

Uniform random numbers are used to define three axial lengths of a marker ellipsoid whose axial ratio was given. The

Table 2 Value of χ^2 of all the models calculated within the defined region where the freedom is 7. Normal distribution is assumed.

model	value of χ^2	defined region
model 1	2.38077	[1,4]
model 2	2.38077	[1,3.4]
model 3	2.38077	[1,2.5]
model 4	2.38077	[1,1.6]
model 5	2.78618	[1,5]
model 6	1.31431	[2,8]
model 7	1.31431	[7,13]
model 8	2.57679	[1,4]
model 9	2.50172	[1,4]
model 10	2.62299	[1,4]

Table 3 Value of χ^2_α. χ^2_α is the value of χ^2 where the level of significance α changes from 0.99 to 0.005 and the freedom is 7.

level of significance α	value of χ^2_α
0.99	1.24
0.95	2.17
0.90	2.83
0.75	4.25
0.50	6.35
0.25	9.04
0.1	12.02
0.05	14.07
0.01	18.48
0.005	20.3

χ^2 tests are performed for the uniform random number where the defined region is [0,1] and the freedom is 9.

The χ^2 values for four sample sizes are calculated as follows. Four tests are enough in this case because the region of variable is fixed.

χ^2=3.6 at n=100.

χ^2=3.4 at n=300.

χ^2=3.0 at n=600.

χ^2=2.96 at n=1000.

The χ^2_α value where the level of significance α varies from 0.99 to 0.005 and the freedom is 9, are indicated on Table 4.

It is clear from the table that the χ^2 values calculated for four sample sizes are small enough compared to the χ^2_α values. The uniform random numbers thus produced are well random to use for the present simulation.

Table 4 Value of χ^2_α where α varies from 0.99 to 0.005 and the freedom is 9.

level of significance α	value of χ^2_α
0.99	2.09
0.95	3.33
0.90	4.17
0.75	5.90
0.50	8.34
0.25	11.39
0.1	14.68
0.05	16.92
0.01	21.7
0.005	23.6

A.3. Randomness test of the principal direction of the initial marker ellipsoids (by Woodcock and Naylor's randomness test)

It is examined whether the principal direction of the initial marker ellipsoids is random or not by the method developed by Woodcock and Naylor (1983). The randomness test is performed for four sample sizes, 100, 300, 600 and 1000. The $\frac{S_1}{S_3}$ values for X, Y and Z axes in each case are shown on Table 5a where $\frac{S_1}{S_3}$ is denoted as $S13$. The critical values of $\frac{S_1}{S_3}$ that were calculated by Woodcock and Naylor (1983) are also shown on Table 5b. It can be said by comparing both tables that the principal direction of the initial marker ellipsoids is random for every sample size.

A.4. Randomness test of the principal direction of the initial marker ellipsoids (by the calculation of fabric ellipse)

Table 5 Woodcock and Naylor's randomness test.

a : $\frac{S_1}{S_3}$ value of X, Y and Z axes for each sample size 100, 300, 600 and 1000. $S13$ means $\frac{S_1}{S_3}$. b : Critical value of $\frac{S_1}{S_3}$ for each sample size 100, 300, 600 and 1000 (Woodcock and Naylor,1983).

sample size (n)	S13 value of X	S13 value of Y	S13 value of Z
100	1.34601	1.23464	1.31795
300	1.16250	1.11528	1.20014
600	1.10568	1.04090	1.07448
1000	1.08414	1.07467	1.05081

sample size (n)	confidence level 90%	confidence level 95%	confidence level 97.5%	confidence level 99%
100	1.597	1.667	1.736	1.82
300	1.30	1.34	1.38	1.44
600	1.20	1.23	1.26	1.29
1000	1.161	1.177	1.192	1.207

If the principal direction of initial marker ellipsoids distributes randomly, their fabric ellipsoid becomes a sphere. In other words three axial lengths of the fabric ellipsoid are unity. The axial lengths of all the fabric ellipsoids before deformation in every model are shown on Table 6. Since these fabric ellipsoids are close to a sphere as shown on the table, the principal direction of the initial marker ellipsoids in every model is close to random.

Table 6 Axial lengths of fabric ellipsoid of all models at undeformed state.

model	length of X	length of Y	length of Z
model 1	1.04754	1.01631	0.939302
model 2	1.03808	1.01450	0.949549
model 3	1.02377	1.01056	0.966573
model 4	1.00952	1.00484	0.985791
model 5	1.06502	1.02047	0.920114
model 6	1.13885	1.01917	0.861556
model 7	1.25971	0.965869	0.821886
model 8	1.01575	1.00447	0.980116
model 9	1.01487	0.998628	0.986702
model 10	1.01439	0.993851	0.991917

References

Cloos, E. (1947) Oolite deformation in the southern mountain fold, Maryland. *Geol. Soc. Am. Bull.* , vol. 58, pp. 843-918.

Couzens, B. A. and Dunne, W. M. (1994) Displacement transfer at thrust terminations: the Saltville thrust and Sinking Creek anticline, Virginia, U.S.A. *J. Struct. Geol.* , vol. 16, no. 6, pp. 781-793.

Dunnet, D. (1969) A technique of finite strain analysis using elliptical particles. *Tectonophysics*, vol. 7, pp. 117-136.

Dunnet, D. and Siddans, A. W. B. (1971) Non-random sedimentary fabrics and their modification by strain. *Tectonophysics*, vol. 12, pp. 307-325.

Elliott, D. (1970) Determination of finite strain and initial shape from deformed elliptical objects. *Geol. Soc. Am. Bull.*, vol. 81, pp. 2221-2236.

Fry, N. (1979) Random point distributions and strain measurement in rocks. *Tectonophysics*, vol. 60, pp. 89-105.

Hayashi, D. (1988) Three dimensional finite strain analysis - with reference to Kayo Formation, Kunchan Group, Okinawa-jima -. *J. Geol. Soc. Japan*, vol. 94, no. 10, pp. 757-768. (in Japanese with English abstract)

Hayashi, D. (1989) Correction of errors in "Three dimensional finite strain analysis - with reference to Kayo Formation, Kunchan Group, Okinawa-jima - Hayashi, 1988" . *J. Geol. Soc. Japan*, vol. 95, no. 7, pp. 553-558. (in Japanese with English abstract)

Hayashi, D. (1995) Proposed consistency c-value for strain ellipsoids in geological structure analysis. *Geoinformatics*, vol. 6, no. 1, pp. 13-29. (in Japanese with English abstract)

Helm, D. G. and Siddans, A. W. B. (1971) Deformation of a slaty, lapillar tuff in the English Lake District: Discussion. *Geol. Soc. Amer. Bull.*, vol.82, pp. 523-531.

Lacassin, R. and van den Driessche, J. (1983) Finite strain determination of gneiss:application of Fry' s method to porphyroid in the southern Massif Central (France). *J. Struct. Geol.*, vol. 5, no. 3/4, pp. 245-253.

Lisle, R. J. (1977) Clastic grain shape and orientation in relation to cleavage from the Aberystwyth grits, Wales. *Tectonophysics*, vol. 39, pp. 381-395.

Lisle, R. J. (1984) Strain discontinuities within the Seve-Koli Nappe Complex, Scandinavian Caledonides. *J. Struct. Geol.*, vol. 6, no. 1/2, pp. 101-110.

Lisle, R. J. (1985) *Geological strain analysis ; A manual for the R_f/ϕ method.* Pergamon, Oxford, 99p.

McKenzie, D. and Jackson, J. (1983) The relationship between strain rates, crustal thickening, paleomagnetism, finite strain and fault movements within a deforming zone. *Earth Planet. Sci. Lett.*, vol.65, pp. 182-202.

Matthews, P. E. , Bond, R. A. B. and Van Den Berg, J. J. (1974) An algebraic method of strain analysis using elliptical markers. *Tectonophysics*, vol. 24, pp. 31-67.

Oertel, G. (1970) Deformation of a slaty, lapillar tuff in the Lake District, England. *Geol. Soc. Amer. Bull.*, vol. 81, pp. 1173-1188.

Panozzo, R. (1984) Two-dimensional strain from the orientation of lines in a plane. *J. Struct. Geol.*, vol.6, no. 1/2, pp. 215-221.

Ramberg, H. (1975) Particle paths, displacement and progressive strain applicable to rocks. *Tectonophysics*, vol.28, pp. 1-37.

Ramsay, J. G. (1967) *Folding and fracturing of rocks*. McGraw-Hill, New York, 568p.

Sanderson, D. J. (1977) The analysis of finite strain using lines with an initial random orientation. *Tectonophysics*, vol.43, pp. 199-211.

Shimamoto, T. and Ikeda, Y. (1976) A simple algebraic method for strain estimation from deformed ellipsoidal objects. 1. Basic theory. *Tectonophysics*, vol.36, pp. 315-337.

Siddans, A. W. B. (1980) Analysis of three-dimensional, homogeneous, finite strain using ellipsoidal objects. *Tectonophysics*, vol. 64, pp. 1-16.

Tikoff, B. and Fossen, H. (1993) Simultaneous pure and simple shear: the unifying deformation matrix. *Tectonophysics*, vol.217, pp.267-283.

Truesdell, C. (1953) Two measures of vorticity. *J. Rational* Mech. Anal., vol. 2, pp. 173-217.

Wheeler, J. (1986) Average properties of ellipsoidal fabrics: implications for two- and three- dimensional methods of strain analysis. Tectonophysics, vol. 126, pp. 259-270.

Woodcock, N. H. and Naylor, M. A. (1983) Randomness testing in three-dimensional orientation data. *J. Struct. Geol.*, vol. 5, no. 5, pp. 539-548.

要　旨

楕円体パッシブマーカーを用いた3次元歪み解析の精度に影響する因子

：林　大五郎

passiveな楕円体の歪マーカーを用いた平均法による3次元歪解析の精度が、初期歪マーカー楕円体の軸比が正規分布する場合に、3つの因子 (1) マーカーの数 (2) マーカーの軸比の平均 (3) マーカーの軸比の標準偏差、とどう関係しているかを調べた。変形場としては (i) 純粋剪断 (ii) 体積変化のないtranspression (iii) 単純剪断、の3つを仮定した。結果は (1) 歪マーカーの数が多いほど歪解析の精度が高い。しかし歪マーカーの数が300をこえると精度に変化はない。(2) 歪マーカーの軸比の平均が1に近いほど、歪解析の精度は高い。(3) 歪マーカーの軸比の標準偏差が小さいほど歪解析の精度は高い。これらの結果は3つの変形場でほぼ同様に成立する。しかしtranspressionと単純剪断では、変形につれ歪解析の精度は高くなるが、純粋剪断では変形につれて精度は変化しない。

キーワード：精度、3次元歪解析、楕円体パッシブマーカー、平均法